

https://doi.org/10.1070/QEL16663

Resonant dipole–dipole interaction of Rydberg atoms for realisation of quantum computations

I.I. Beterov, G.N. Khamzina, D.B. Tret'yakov, V.M. Entin, E.A. Yakshina, I.I. Ryabtsev

Abstract. **We report the application of the resonant dipole–dipole interaction of Rydberg atoms for the realisation of quantum computations with ultracold neutral atoms. Coherent population oscillations between the collective states of systems consisting of two interacting atoms make it possible to implement two-qubit phase gates, which are necessary for universal quantum computations. The schemes studied are alternatives to two-qubit gates based on the Rydberg dipole blockade effect. In contrast, the schemes we propose do not require large dipole–dipole interaction energies and can be realised for atoms that are at a considerable distance from each other.**

Keywords: *Rydberg atoms, quantum computations, adiabatic passage.*

1. Introduction

Considerable progress has been recently made in the experimental realisation of quantum computations [1]. The most important recent achievements are related to the creation of quantum registers consisting of 50 separate qubits, two-level quantum systems, based on Josephson tunneling in superconductors [2]. At the same time, the accuracy of two-qubit operations in such systems remains insufficiently low, and scaling to a large number of qubits while maintaining individual addressing is quite a challenge [3]. The high accuracy of two-qubit operations is demonstrated with ultracold ions in radio-frequency electric traps [4, 5]. Yet, the scaling of quantum registers consisting of ions is also hampered by complex oscillations of the ion chain [6].

In this connection, ultracold neutral atoms are of particular interest for creating a large-scale quantum register [7–9]. Recently, one-dimensional, two-dimensional and three-dimensional arrays of optical dipole traps loaded with single ultracold alkali metal atoms with individual addressing to each individual atom have been demonstrated [10–13]. An example of a two-dimensional array of optical dipole traps is shown in Fig. 1a. The logical states of qubits are long-lived hyperfine sublevels of the ground state of atoms, which ensure a long-term storage of quantum information [7, 9].

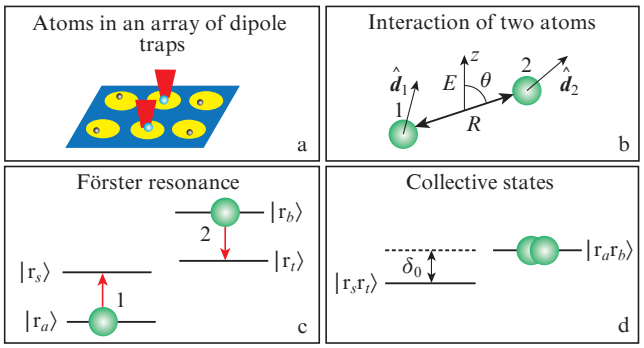

Figure 1. (a) Scheme of a quantum register consisting of single ultracold neutral atoms trapped in an array of optical dipole traps with individual addressing to each individual atom by focused laser radiation, (b) dipole–dipole interaction of two Rydberg atoms (the quantisation axis is directed along the external electric field), (c) Förster resonances for two interacting Rydberg atoms and (d) detuning from the Förster resonance for the transition between the collective states $|r_a, r_b\rangle$ and $|r_s, r_t\rangle$.

The methods of initialising the initial quantum state of the register with the use of optical pumping and optical detection of quantum states of qubits by the resonance fluorescence signal have been successfully implemented. Accurate single-qubit gates are demonstrated using resonant microwave radiation that induces magnetic dipole transitions between hyperfine sublevels of the ground state of alkali metal atoms. The individuality of addressing to individual qubits is achieved by irradiating individual atoms with focused nonresonant laser radiation. Due to the light shift arising in the field of such radiation, the energy levels of the chosen qubit are tuned to the resonance with microwave radiation [11].

The main difficulty preventing the creation of quantum computers based on ultracold neutral atoms is the comparatively low accuracy of the two-qubit gates. For their implementation, use can be made of the Rydberg dipole blockade effect [14] when, upon irradiation of two atoms by resonant laser radiation exciting Rydberg energy levels, there occurs a collective energy level shift due to a strong interatomic inter-

I.I. Beterov A.V. Rzhanov Institute of Semiconductor Physics, Siberian Branch, Russian Academy of Sciences, prosp. Akad. Lavrent'eva 13, 630090 Novosibirsk, Russia; Novosibirsk State University, ul. Pirogova 2, 630090 Novosibirsk, Russia; Novosibirsk State Technical University, prosp. Karla Marksa 20, 630073 Novosibirsk, Russia;
e-mail: beterov@isp.nsc.ru;
G.N. Khamzina A.V. Rzhanov Institute of Semiconductor Physics, Siberian Branch, Russian Academy of Sciences, prosp. Akad. Lavrent'eva 13, 630090 Novosibirsk, Russia; Novosibirsk State Technical University, prosp. Karla Marksa 20, 630073 Novosibirsk, Russia;
D.B. Tret'yakov, V.M. Entin, E.A. Yakshina, I.I. Ryabtsev A.V. Rzhanov Institute of Semiconductor Physics, Siberian Branch, Russian Academy of Sciences, prosp. Akad. Lavrent'eva 13, 630090 Novosibirsk, Russia; Novosibirsk State University, ul. Pirogova 2, 630090 Novosibirsk, Russia

Received 21 February 2018
Kvantovaya Elektronika **48** (5) 453–459 (2018)
Translated by I.A. Ulitkin

action, for which both atoms are in the Rydberg state. With a sufficient strong interaction (for example, much higher than the Rabi frequency of laser excitation), such collective energy levels are expelled from resonance with laser radiation and the simultaneous excitation of two Rydberg atoms becomes impossible. As a result, a system of two interacting atoms turns out to be in an entangled collective state containing only one Rydberg excitation. This can be used to implement two-qubit 'controlled-Z' (CZ) and 'controlled-NOT' (CNOT) gates. Despite the fact that, according to theoretical calculations, the accuracy of such quantum operations can reach 99.99% [15], the experimentally measured accuracy does not exceed 73% [16].

This can be due to a number of reasons. The Rydberg energy levels are extremely sensitive to parasitic electric fields (their polarisabilities increase with increasing principal quantum number n as n^7). The complex structure of the Stark sublevels of strongly interacting Rydberg atoms can lead to partial or complete destruction of the dipole blockade and to a loss of coherence during laser excitation. In this connection, of interest are alternative schemes for the implementation of two-qubit gates that do not require a high dipole–dipole interaction energy. Such schemes can make use of electrically tunable Förster resonances, which have been demonstrated and investigated in a number of experiments [17–21].

In this paper, we consider schemes of two-qubit gates based on a resonant dipole–dipole interaction. In the first scheme, a coherent dipole–dipole interaction of rubidium atoms is used in the conditions of an exact Förster resonance tuned by an electric field. The accuracy of the two-qubit gate is estimated taking into account the finite lifetimes of Rydberg states and the influence of nearby Rydberg levels. The second scheme uses the adiabatic passage of the Förster resonances in a time-dependent electric field. Adiabatic passage allows the quantum gate accuracy sensitivity to interatomic distance fluctuations to be reduced.

2. Förster resonances tuned by the electric field

Consider the interaction of two Rydberg atoms located at a distance R from each other, as shown in Fig. 1b. We choose the quantisation axis z coinciding with the direction of the external control electric field E. Let θ be the angle between the quantisation axis and the vector connecting the atoms. The dipole–dipole interaction operator of atoms is described by expression

$$V_{\rm dd} = \frac{1}{4\pi\varepsilon_0 R^3}(\hat{\boldsymbol{d}}_1\hat{\boldsymbol{d}}_2 - 3(\hat{\boldsymbol{d}}_1\boldsymbol{n})(\hat{\boldsymbol{d}}_2\boldsymbol{n})). \quad (1)$$

Here, $\hat{\boldsymbol{d}}_1$ and $\hat{\boldsymbol{d}}_2$ are the dipole moment operators for atoms 1 and 2; $\boldsymbol{n}$ is the unit vector connecting the atoms; and ε_0 is the dielectric constant. We write equation (1) in the following form convenient for calculations:

$$\begin{aligned}\hat{V}_{\rm dd} = \frac{1}{4\pi\varepsilon_0 R^3}[&S_1(\theta)(\hat{d}_{1+}\hat{d}_{2-} + \hat{d}_{1-}\hat{d}_{2+} + 2\hat{d}_{1z}\hat{d}_{2z})\\ &+ S_2(\theta)(\hat{d}_{1+}\hat{d}_{2z} - \hat{d}_{1-}\hat{d}_{2z} + \hat{d}_{1z}\hat{d}_{2+} - \hat{d}_{1z}\hat{d}_{2-})\\ &- S_3(\theta)(\hat{d}_{1+}\hat{d}_{2+} + \hat{d}_{1-}\hat{d}_{2-})]. \quad (2)\end{aligned}$$

Here, $\hat{d}_{k,\pm} = \mp(\hat{d}_{k,x} \pm i\hat{d}_{k,y})/\sqrt{2}$ are the components of the dipole moment operator in a spherical basis, and

$$\begin{aligned}S_1(\theta) &= \frac{1-3\cos^2\theta}{2},\\ S_2(\theta) &= \frac{3\sin\theta\cos\theta}{\sqrt{2}}, \quad (3)\\ S_3(\theta) &= \frac{3\sin^2\theta}{2}\end{aligned}$$

are the angular factors. The dipole–dipole interaction described by the operator $\hat{V}_{\rm dd}$ leads to transitions between the collective Rydberg states of two interacting atoms $|{\rm r}_a, {\rm r}_b\rangle \to |{\rm r}_s, {\rm r}_t\rangle$, as shown in Fig. 1c, where for the state of each individual atom $|{\rm r}\rangle = |nljm_j\rangle$ (n is the principal quantum number, l is the orbital angular momentum, j is the total angular momentum, and m_j is the projection of the total angular momentum on the z axis). The matrix element of the operator is described by the expression [22]:

$$\begin{aligned}\langle n_s m_s l_s j_s; n_t m_t l_t j_t|\hat{V}_{\rm dd}|n_a m_a l_a j_a; n_b m_b l_b j_b\rangle = \frac{e^2}{4\pi\varepsilon_0 R^3}\\ \times \Big\{S_1(\theta)\Big[2C^{j_s m_s}_{j_a m_a 10}C^{j_t m_t}_{j_b m_b 10} + C^{j_s m_s}_{j_a m_a 11}C^{j_t m_t}_{j_b m_b 1-1}\\ + C^{j_s m_s}_{j_a m_a 1-1}C^{j_t m_t}_{j_b m_b 11}\Big] + S_2(\theta)\Big[\Big(C^{j_s m_s}_{j_a m_a 11} - C^{j_s m_s}_{j_a m_a 1-1}\Big)\\ \times C^{j_t m_t}_{j_b m_b 10} + C^{j_s m_s}_{j_a m_a 10}\Big(C^{j_t m_t}_{j_b m_b 11} - C^{j_t m_t}_{j_b m_b 1-1}\Big)\Big]\\ - S_3(\theta)\Big[C^{j_s m_s}_{j_a m_a 11}C^{j_t m_t}_{j_b m_b 11} + C^{j_s m_s}_{j_a m_a 1-1}C^{j_t m_t}_{j_b m_b 1-1}\Big]\Big\}\\ \times \sqrt{\max(l_a,l_s)}\sqrt{\max(l_b,l_t)}\sqrt{(2j_a+1)(2j_b+1)}\\ \times \begin{Bmatrix} l_a & 1/2 & j_a\\ j_s & 1 & l_s\end{Bmatrix}\begin{Bmatrix} l_b & 1/2 & j_b\\ j_t & 1 & l_b\end{Bmatrix}\\ \times (-1)^{l_s+\frac{l_a+l_s+1}{2}}(-1)^{l_t+\frac{l_b+l_t+1}{2}}(-1)^{j_a+j_b}R^{n_s l_s}_{n_a l_a}R^{n_t l_t}_{n_b l_b}. \quad (4)\end{aligned}$$

Here, $R^{n_s l_s}_{n_a l_a}$ and $R^{n_t l_t}_{n_b l_b}$ are the radial matrix elements for the transitions $|n_a l_a\rangle \to |n_s l_s\rangle$ and $|n_b l_b\rangle \to |n_t l_t\rangle$, respectively. We calculated the matrix elements using the quasi-classical approximation and the quantum defect method [23].

The dipole–dipole interaction operator $\hat{V}_{\rm dd}$ relates the collective states of two interacting atoms for which the total magnetic quantum number $M = m_1 + m_2$ changes by $\Delta M = 0, \pm 1, \pm 2$.

The collective energy levels of the two interacting atoms are shown schematically in Fig. 1d. The energy difference between the collective states is determined as:

$$\hbar\delta_0 = [U({\rm r}_a) - U({\rm r}_s)] + [U({\rm r}_b) - U({\rm r}_t)]. \quad (5)$$

In the case when these levels are degenerate, i.e., $\delta_0 = 0$, the Förster resonance is observed, which manifests itself as a significant increase in the probability of a transition between such states. The value of δ_0 is the energy defect, or detuning from the Förster resonance. To tune the energy levels to the exact resonance, one can use an external electric field. Figure 2a shows a numerically calculated Stark diagram of the energy levels of rubidium in an external electric field for the states with the projection of the total angular momentum of the atom $|m| = 1/2$ onto the electric field direction. Figure 2b demonstrates the numerically calculated collective energy levels $|70{\rm S}_{1/2}, 73{\rm S}_{1/2}\rangle$ and $|70{\rm P}_{1/2}, 72{\rm P}_{1/2}\rangle$ in an external electric field. The Förster resonance corresponds to the intersection of these levels and is observed in an electric field with 0.222 V cm^{-1}.

The choice of this particular resonance is due to the fact that in its vicinity the Stark effect for Rydberg nS states retains, as can be seen from Fig. 2, a quadratic character. The quadratic character of the Stark effect is necessary to ensure that the working levels do not intersect with a hydrogen-like set of a large number of states experiencing the linear Stark effect (Fig. 2a) and that the accuracy of quantum operations increases. For higher states, the search for such resonances is a challenging task.

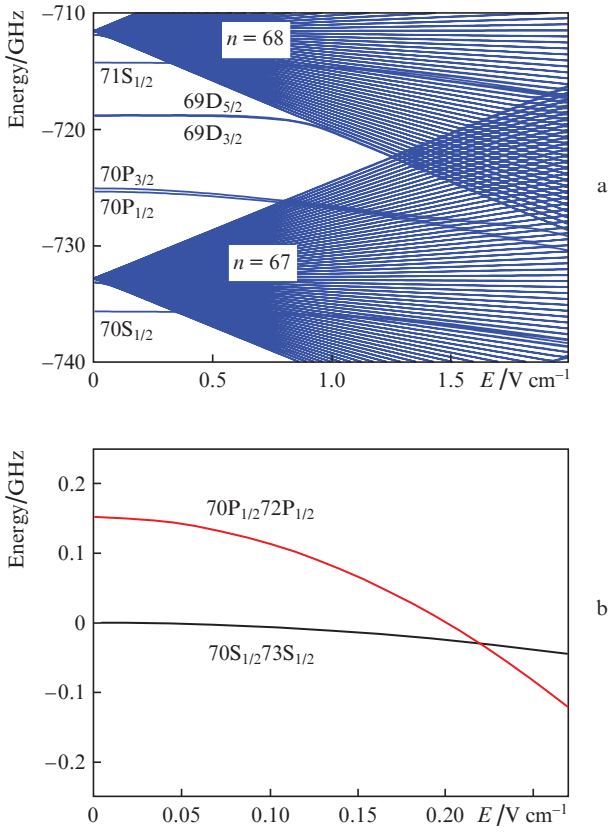

Figure 2. (a) Numerically calculated Stark diagram of Rydberg rubidium atoms in an external electric field for states with the projection of the total angular momentum of the atom $|m| = 1/2$ in the direction of the electric field and (b) collective energy levels $|70S_{1/2}, 73S_{1/2}\rangle$ and $|70P_{1/2}, 72P_{1/2}\rangle$ in an external electric field (the Förster resonance corresponds to the intersection of these levels and is observed in an electric field of 0.222 V cm^{-1}).

3. Two-qubit operations using coherent resonant dipole–dipole interaction

In the case of an exact Förster resonance, coherent oscillations of populations of collective states $|r_a, r_b\rangle$ and $|r_s, r_t\rangle$ are observed for two stationary Rydberg atoms, analogous to the Rabi oscillations in a two-level quantum system interacting with resonant radiation. Similar oscillations were experimentally recorded in [24]. One can choose such a duration of interaction that the system of two interacting atoms will return to the initial state, acquiring a phase shift of their collective wave function. In this case, use can be made of a two-qubit CZ gate, as shown in Fig. 3a.

Atom 1 is excited to the Rydberg state $|r_a\rangle$ by a laser π-pulse, denoted by 1. Atom 2 is excited to the Rydberg state $|r_b\rangle$ by a laser π-pulse, denoted by 2. These π-pulses must ensure a complete population transfer from the initial states of the atoms to the final states. Pulses 1 and 2 can be either simultaneous or spaced in time. Atoms are located far enough

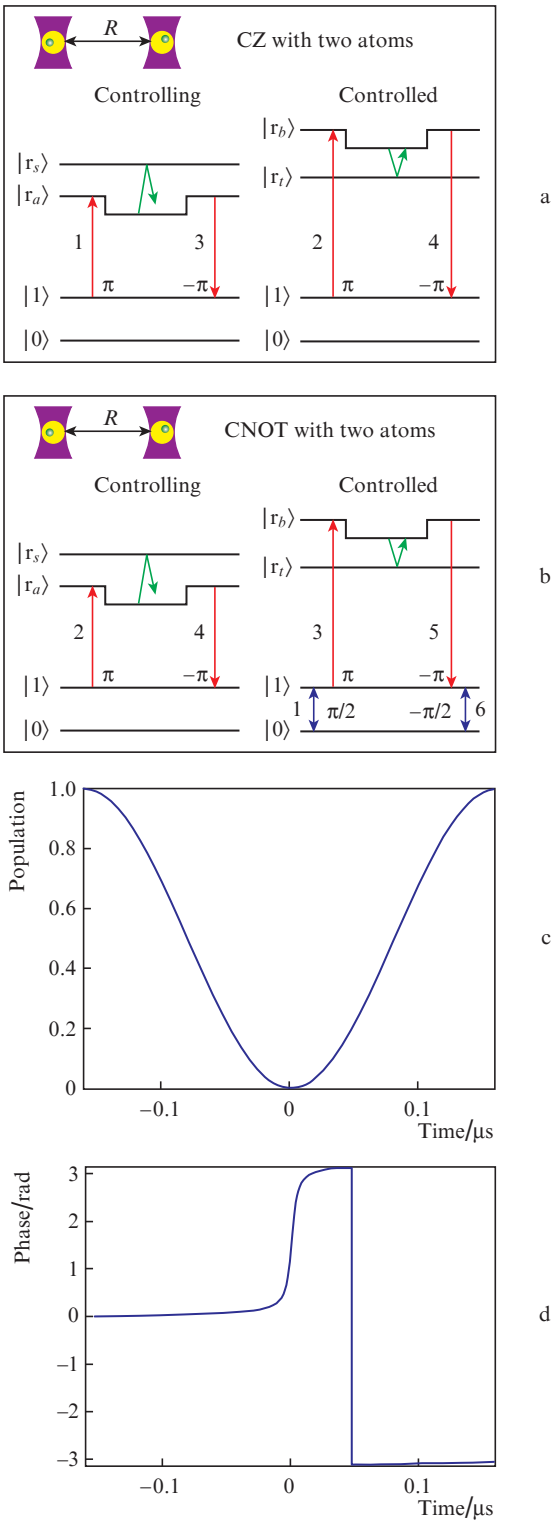

Figure 3. Schemes of two-qubit (a) CZ and (b) CNOT gates using the resonance dipole–dipole interaction, as well as numerically calculated time dependences of the (c) population and (d) phase of the initial collective state $|70S_{1/2}, 73S_{1/2}\rangle$ under conditions of the resonance dipole–dipole interaction with the state $|70P_{1/2}, 72P_{1/2}\rangle$.

from each other, so that the van der Waals interaction between them does not lead to a dipole blockade of the Rydberg excitation (in the absence of an external electric field, the Förster resonance has a large detuning, and so the interaction will be van der Waals). Then, after switching on an electric field, it adjusts the collective energy levels to the Förster resonance, which now corresponds to a resonant dipole–dipole interaction. After some time the system passes from the state $|r_a, r_b\rangle$ to the state $|r_s, r_t\rangle$, and then returns to the initial state, acquiring a phase shift π, which is equivalent to the action of the 2π-pulse in the two-level system. After that, the external electric field is turned off and the atoms are de-excited by laser $-\pi$-pulses 3 and 4, whose optical phases with respect to pulses 1 and 2, respectively, should be selected so that in the absence of dipole–dipole interaction, each atom returns to its original state without a phase shift.

This scheme can be modified for the CNOT gate (see Fig. 3b). Thus, before and after the CZ operation, one-qubit rotations of the state vector of the controlled qubit are performed around the y axis by an angle of $\pi/2$ in opposite directions. A train of pulses acting on the controlled qubit leaves its state unchanged if the controlling qubit is not excited to the Rydberg state and the dipole–dipole interaction does not lead to a phase shift. Otherwise, the state of the controlled qubit will be inverted, which is required for the implementation of the CNOT gate.

We have numerically simulated the population dynamics (normalised to unity, Fig. 3c) and phases (Fig. 3d) of the collective states for the Förster resonance $|70S_{1/2}, 73S_{1/2}\rangle \leftrightarrow |70P_{1/2}, 72P_{1/2}\rangle$ in rubidium atoms located at a distance of 15.5 μm from each other in a resonant electric field of 0.222 V cm^{-1}. The electric field was directed along the vector connecting the atoms. It allowed us to limit all possible transitions between those collective states for which $\Delta M = 0$. In the calculations we took into account all the Stark sublevels for the resonance $|70S, 73S\rangle \leftrightarrow |70P, 72P\rangle$. Since the phase values are in the range $(-\pi, \pi)$, accumulation of the dynamic phase leads a phase jump, $\pi \to -\pi$, as shown in Fig. 3d. Previously, we dis-

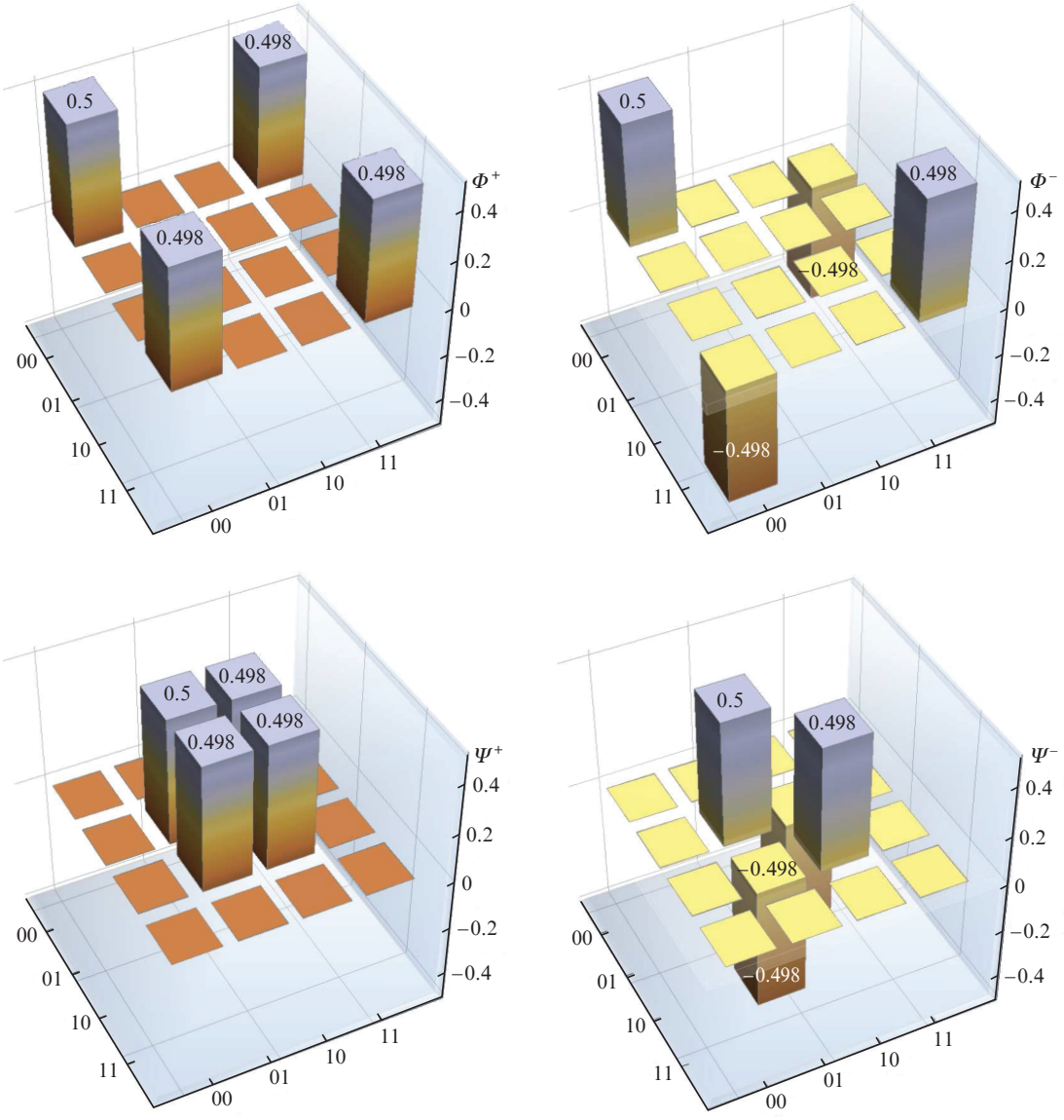

Figure 4. Numerically calculated density matrices of quantum-entangled Bell states for rubidium atoms obtained using the coherent dipole–dipole interaction of Rydberg atoms.

covered that nonresonant excitation channels result in phase errors that reduce the accuracy of two-qubit gates [24]. Therefore, in order to estimate the accuracy of the two-qubit gates, we performed a numerical simulation of the generation of quantum-entangled Bell states taking into account the lifetime of the Rydberg levels [25] and the dipole–dipole interaction of atoms during laser excitation. In our calculations the laser excitation was assumed to occur under conditions of a zero electric field. The entangled Bell states are described by the following wave functions:

$$\Phi^+ = \frac{1}{\sqrt{2}}(|00\rangle + |11\rangle),$$

$$\Phi^- = \frac{1}{\sqrt{2}}(|00\rangle - |11\rangle),$$

$$\Psi^+ = \frac{1}{\sqrt{2}}(|01\rangle + |10\rangle),$$

$$\Psi^- = \frac{1}{\sqrt{2}}(|01\rangle - |10\rangle). \quad (6)$$

Numerically calculated density matrices of Bell states are shown in Fig. 4. These calculations show that the accuracy of their generation is rather high and reaches 96%.

4. Adiabatic passage of Förster resonances tuned by the electric field

An important factor that reduces the accuracy of quantum gates based on a resonant dipole–dipole interaction is the fluctuations in the distance between the atoms trapped in optical dipole traps. To reduce their influence, use can be made of a double adiabatic passage of the Förster resonances in a time-dependent electric field [26, 27]. To this end, we modified the scheme of the two-qubit CZ gate, as shown in Fig. 5a. In paper [26] we considered this two-qubit gate with caesium

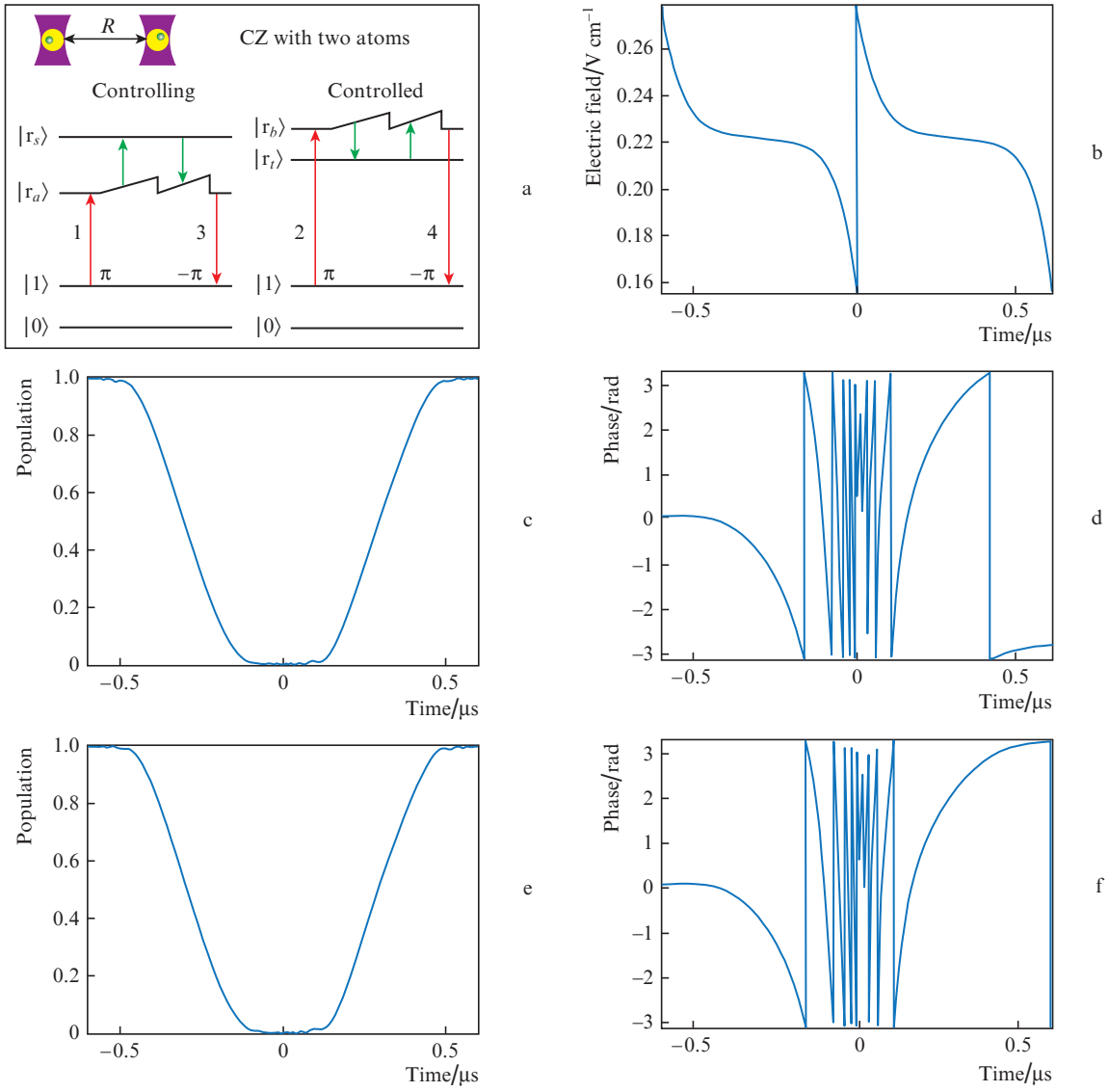

Figure 5. (a) Scheme of a two-qubit CZ gate using the double adiabatic passage of the Förster resonances tuned by the electric field and (b) time dependence of the electric field for the adiabatic passage of the Förster resonances, as well as numerically calculated dynamics of (c) population and (d) phase of the initial state $|70S_{1/2}, 73S_{1/2}\rangle$ under double adiabatic passage and numerically calculated dynamics of (e) population and (f) phase of the state $|70S_{1/2}, 73S_{1/2}\rangle$ under double adiabatic passage with phase correction.

atoms, and then modified this scheme for the Förster resonances induced by the radio-frequency electric field [27].

Due to the Stark effect, the time-dependent electric field shifts the collective energy levels so that the system passes twice through the Förster resonance, $|70S_{1/2}, 73S_{1/2}\rangle \leftrightarrow |70P_{1/2}, 72P_{1/2}\rangle$. Due to the resonance dipole–dipole interaction, the system undergoes transition from the initial state $|70S_{1/2}, 73S_{1/2}\rangle$ to the final state $|70P_{1/2}, 72P_{1/2}\rangle$, and then returns back, acquiring the deterministic phase shift π.

In [26, 27], we showed that for an accurate fast adiabatic passage in the case when the interaction energy is independent of time, it is necessary to use the nonlinear dependence of the resonance detuning on time. In the calculations, we used the following dependence of the Förster resonance detuning on time:

$$\delta_0(t) = \begin{cases} s_1(t - t_1) + s_2(t - t_1)^5, & t \leqslant 0, \\ s_1(t - t_2) + s_2(t - t_2)^5, & t > 0. \end{cases} \quad (7)$$

Here, $s_1/2\pi = 22.6$ MHz μs^{-1}; $s_2/2\pi = 28800$ MHz μs^{-5}; and $t_1 = -0.3$ μs and $t_2 = 0.3$ μs. Figure 5b shows the time dependence of the electric field that tunes the Förster resonance $|70S_{1/2}, 73S_{1/2}\rangle \leftrightarrow |70P_{1/2}, 72P_{1/2}\rangle$ in accordance with equation (6). The numerically calculated dependences of the population and phase of the initial state $|70S_{1/2}, 73S_{1/2}\rangle$ are shown in Figs 5c and 5d, respectively. Nonresonant excitation channels result both in a small leakage of the population and in the appearance of phase errors, which can be partly corrected by a change in the dependence of the electric field on time, for example, by changing $t_2 = 0.2993$ μs. The numerically calculated dependences of the population and phase of the state $|70S_{1/2}, 73S_{1/2}\rangle$ with phase error correction are shown in Figs 5e and 5f, respectively. Correction of phase errors makes it possible to compensate for the effect of nonresonant excitation channels only for a certain distance between the atoms. When the distance is changed, such errors arise again.

To estimate the influence of fluctuations of the interatomic distance on the error of two-qubit gates, we compared in Fig. 6 the accuracy of the numerically calculated Bell states as a function of the distance between the atoms for two different schemes of two-qubit gates – using coherent population oscillations and double adiabatic passage. Adiabatic passage requires more time to implement two-qubit gates compared to a coherent dipole–dipole interaction at the same distance between the atoms. This leads to an increase in the contribution of the finite lifetimes of the Rydberg states to errors in the generation of Bell states. Despite this, it can be seen that the use of double adiabatic passage with phase correction makes it possible to obtain a higher accuracy of the generation of Bell states and to reduce the sensitivity to fluctuations in the interatomic distance. The minimum error of the generation of Bell states in our calculations was 0.7%.

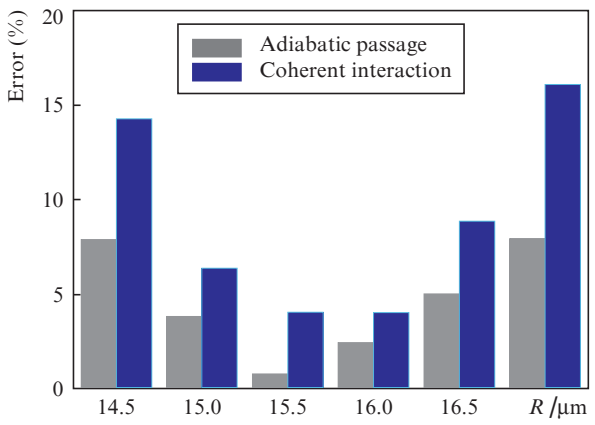

Figure 6. Dependences of the error of the generation of Bell states on the distance between the atoms for two-qubit gates using the coherent dipole–dipole interaction and double adiabatic passage.

5. Conclusions

We have considered the schemes of two-qubit gates based on a resonant dipole–dipole interaction of ultracold Rydberg rubidium atoms. The accuracy of the generation of quantum-entangled Bell states has been shown to be increased by using the double adiabatic passage of the Förster resonances tuned by the electric field.

The main sources of errors in the implementation of two-qubit gates are the finite lifetimes of the Rydberg states, phase errors and population leakage due to nonresonant excitation channels, as well as a possible violation of the adiabatic regime during double adiabatic passage. The experimental realisation of the proposed schemes requires a precise control of the electric fields in which the Rydberg atoms are located.

Acknowledgements. The study of the accuracy of the generation of Bell states was supported by the Russian Science Foundation (Grant No. 16-12-00028). The work was also supported by the Russian Foundation for Basic Research (Grant Nos 16-02-00383 and 17-02-00987), the Novosibirsk State University and the Russian Academy of Sciences.

References

1. Nielsen M.A., Chuang I.L. *Quantum Computation and Quantum Information* (Cambridge: Cambridge University Press, 2011).
2. https://www.research.ibm.com/ibm-q/.
3. Gambetta J.M., Chow J.M., Steffen M. *Nature Partner J. Quantum Inform.*, **3**, 2 (2017).
4. Ballance C., Harty T.P., Linke N.M., Sepiol M.A., Lukas D.M. *Phys. Rev. Lett.*, **117**, 060504 (2016).
5. Gaebler J.P., Tan T.R., Lin Y., Wan Y., Bowler R., Keith R.A.C., Glancy S., Coakley K., Knill E., Leibfried D., Wineland D.J. *Phys. Rev. Lett.*, **117**, 060505 (2016).
6. Brown K.R., Kim J., Monroe C. *Nature Partner J. Quantum Inform.*, **2**, 16034 (2016).
7. Saffman M., Walker T.G., Mølmer K. *Rev. Mod. Phys.*, **82**, 2313 (2010).
8. Ryabtsev I.I., Beterov I.I., Tretyakov D.B., Entin V.M., Yakshina E.A. *Usp. Fiz. Nauk*, **176**, 206 (2016).
9. Saffman M. *J. Phys. B: At. Mol. Opt. Phys.*, **49**, 202001 (2016).
10. Bernien H., Schwartz S., Keesling A., Levine H., Omran A., Pichler H., Choi S., Zibrov A.S., Endres M., Greiner M., Vuletić V., Lukin M.D. *Nature*, **551**, 579 (2017).
11. Xia T., Lichtman M., Maller K., Carr A.W., Piotrowicz M.J., Isenhower L., Saffman M. *Phys. Rev. Lett.*, **114**, 100503 (2015).
12. Barredo D., de Léséleuc S., Lienhard V., Lahaye T., Browaeys A. *Science*, **354**, 1021 (2016).
13. Barredo D., Lienhard V., de Léséleuc S., Lahaye T., Browaeys A. ArXiv:1712.02727.
14. Lukin M.D., Fleischhauer M., Cote R., Duan L.M., Jaksch D., Cirac J.I., Zoller P. *Phys. Rev. Lett.*, **87**, 037901 (2001).
15. Theis L.S., Motzoi F., Wilhelm F.K., Saffman M. *Phys. Rev. A*, **94**, 032306 (2016).
16. Maller K.M., Lichtman M.T., Xia T., Sun Y., Piotrowicz M.J., Carr A.W., Isenhower L., Saffman M. *Phys. Rev. A*, **92**, 022336 (2015).
17. Ryabtsev I.I., Tretyakov D.B., Beterov I.I., Entin V.M. *Phys. Rev. Lett.*, **104**, 073003 (2010).

18. Tretyakov D.B., Entin V.M., Yakshina E.A., Beterov I.I., Andreeva C., Ryabtsev I.I. *Phys. Rev. A*, **90**, 041403 (2014).
19. Yakshina E.A., Tretyakov D.B., Entin V.M., Andreeva C., Cinins A., Markovski A., Iftikhar Z., Ekers A., Ryabtsev I.I. *Phys. Rev. A*, **94**, 043417 (2016).
20. Tretyakov D.B., Beterov I.I., Yakshina E.A., Entin V.M., Ryabtsev I.I., Cheinet P., Pillet P. *Phys. Rev. Lett.*, **119**, 173402 (2017).
21. Van Ditzhuijzen C.S.E., Tauschinsky A., van Linden van den Heuvell H.B. *Phys. Rev. A*, **80**, 063407 (2009).
22. Varshalovich D.A., Moskalev A.N., Khersonskii V.K. *Quantum Theory of Angular Momentum* (Singapore: World Scientific, 1988; Leningrad: Nauka, 1975).
23. Kaulakys B. *J. Phys. B: At. Molec. Phys.*, **28**, 4963 (1995).
24. Ravets S., Labuhn H., Barredo D., Beguin L., Lahaye T., Browaeys A. *Nat. Phys.*, **10**, 914 (2014).
25. Beterov I.I., Ryabtsev I.I., Tretyakov D.B., Entin V.M. *Phys. Rev. A*, **79**, 052504 (2009).
26. Beterov I.I., Saffman M., Yakshina E.A., Tretyakov D.B., Entin V.M., Bergamini S., Kuznetsova E.A., Ryabtsev I.I. *Phys. Rev. A.*, **94**, 062307 (2016).
27. Beterov I.I., Hamzina G.N., Yakshina E.A., Tretyakov D.B., Entin V.M., Ryabtsev I.I. ArXiv:1710.04384 (2017).